



**ORIGINAL ARTICLE**

## Mechanical properties of timber-concrete connections with steel tube connectors

Yinyang Liu<sup>a</sup>, Ao Li<sup>a</sup>, Jixing Cao<sup>b,\*</sup>, Dan Yu<sup>c</sup>, Jilu Zhang<sup>c</sup>

<sup>a</sup>School of Civil Engineering, Zhengzhou University, Zhengzhou 450001, China.

<sup>b</sup>Department of Civil & Environmental Engineering, National University of Singapore, Singapore 117576, Singapore.

<sup>c</sup>The Fourth Construction Engineering Company Ltd. of China Construction Second Engineering Bureau, Tianjin 300457, China.

\*Corresponding Author: Jixing Cao. Email: ceecaaj@nus.edu.sg.

**Abstract:** Composite connections are important components of timber-concrete hybrid systems. This work presents a novel shear connector for timber-concrete composite (TCC) connections. To verify the composite action between the timber and concrete in the proposed connection, ten specimens were subjected to push-out tests to examine the slip at the interlayer. The failure mode and maximum load capacity results are analyzed, indicating that the composite connections have good ductility and high load capacity. Four methods to determine the yield point are compared and discussed in detail. According to the test results, a mathematical model is utilized to predict the nonlinear load-slip curve of the proposed connection. The Bayesian method is introduced to estimate the model parameters and quantify the model uncertainty. The obtained results can be used for further reliability analysis. This work demonstrates that timber-concrete connections with novel connectors perform well and show potential for application in composite structures.

**Keywords:** Composite connection; load-slip curve; maximum load-capacity; uncertainty quantification.

### 1 Introduction

The construction industry, including on-site building construction and the demolition of old buildings, has emitted a considerable amount of greenhouse gas and accumulated a considerable amount of construction waste [1-3]. This situation has rapidly exacerbated the conflict between the development of the construction industry and environmental protection. To reduce the impact of construction activities on an environmentally friendly society, an effective solution is to use renewable materials to replace energy-intensive materials [4-5]. For example, some buildings, such as the 18-story Brock Commons in Canada [6] and 14-story “Treet” building in Norway, adopt a timber-concrete hybrid system to take advantage of different material properties [7]. This hybrid structural system has consistently attracted broad attention because it combines the features of wood, including a light weight structure and low carbon emissions, and properties of concrete, including stiffness and fire resistance. For a composite structure, since the stress between different components is transmitted through composite connections, the behavior of composite connections has a significant influence on overall structural performance [8-9]. Thus, it is necessary to comprehensively understand the mechanical properties of timber-concrete composite (TCC) connections.

000017-1



Received: 1 April 2022; Received in revised form: 6 May 2022; Accepted: 16 May 2022  
 This work is licensed under a Creative Commons Attribution 4.0 International License.

Various types of TCC connections have been developed and extensively investigated. The first category of such connections includes those with different indentations in timber [10-11]. Since wood has high tensile strength parallel to the grain and concrete has superior properties in compression, to realize their greatest advantages in strength and stiffness, timber members are usually included in tensile zones, and concrete layers are usually included in compression areas. Boccadoro et al. [12], Shi et al. [13] and Zhang et al. [14] conducted several experimental tests to investigate the mechanical properties of TCC connections with different notch shapes, demonstrating that the notched connection presents a considerable degree of strength and stiffness.

The second category of TCC connections includes those that use shear connectors to ensure composite action. Because environmental change and load conditions have an effect on the creep and shrinkage phenomena of both wood and concrete materials, shear connectors enable the transfer of shear force at the interface and the composite to work effectively. These TCC connections usually include nails or dowels of different diameters [15-17], vertical or inclined screws [18-19], and steel plates [20-21]. The ductility and deformability of this type of connection mainly rely on the deformation capacity of the connectors. For this reason, the ultimate deformation and load capacity should be higher than the maximum slip demand at the interlayer, which allows load redistribution among the connections. This is the basic principle of connections that cannot fail before the failure of the main members.

The above two categories of TCC connections usually require drilling or cutting off the timber so that local force concentrations may occur at the interlayer. To reduce this adverse effect, some researchers have developed adhesive connections [22-23], which use chemical materials to glue the members of timber and concrete together without a metallic fastener. This adhesive technology allows the shear forces to distribute uniformly and reduces the interface slip. However, the properties of the adhesive have a significant effect on the adhesive connection. Various factors, including the short- and long-term behavior of the adhesive [24] and different surface conditions [25], have been experimentally analyzed.

Previous experimental investigations of TCC connections have mainly focused on their mechanical properties. In the design of TCC structures, an analysis model derived from mechanical mechanisms is necessary. The model can be used to analyze the displacement, internal force and ultimate bearing capacity of TCC structures. Because the involved experiment is very expensive, an analysis model calibrated from experimental data is capable of extrapolating some similar cases. Researchers have proposed some useful analysis models [26-27] to predict the load-slip curves. Accompanied by the analytical model, it is usually difficult to determine the model parameters. A common way to obtain the values of parameters involves performing a least square test between experimental data and model predictions [28-29]. Due to model error and measurement noise, model predictions have some uncertainties that need to be quantified. To address this issue, the Bayesian method has been introduced to identify the model parameters associated with uncertainties [30-31]. In this work, a novel connector for TCC connections is proposed. Ten push-out tests are executed to investigate the failure modes and mechanical characteristics of the connections. Based on the test data, a mathematical model is applied to simulate the load-slip curve, whose model parameters are estimated from the probability distribution.

## 2 Material properties

### 2.1 Description of a novel connector

In a TCC structure, the connection is usually designed to have enough ductility to achieve strong deformation before the collapse of the main structure. For such a composite connection, the shear connector plays an important role because it undergoes the shear force between different members. Inclined screws [19], dowels [17,32], and notches [33] are commonly used connectors. Either these connectors are cut or they slip too much. A connector that provides a high degree of stiffness with little slip is needed. In this study, a novel shear connector consisting of a steel tube (**Fig. 1a**) and four screws (**Fig. 1b**) is designed. The steel tube is made of steel material Q235, and the nominal yield strength of Q235 is 235 MPa. Therefore, the steel tube can provide considerable stiffness, while the four embedded screws ensure that the connector has enough shear resistance. Meanwhile, the elongated shape of the

steel tube improves the flexural performance of the connector.

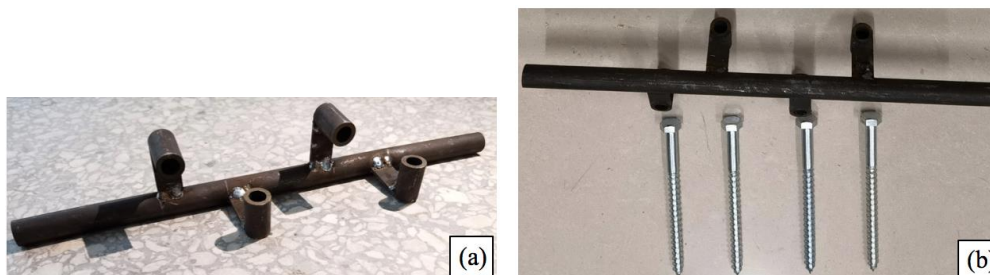


**Fig. 1.** Photographs of a shear connector: (a) Steel tube, (b) Four screws

**Fig. 2a** displays a three-dimensional diagram of the steel tube. The steel tube is made of a long pipe with a length of 300 mm and four 23-mm-long pipes (see **Fig. 2b**). **Fig. 2c** depicts section 1-1 of the pipe, with internal and external diameters of 8 mm and 14 mm, respectively. Each screw has a length of 100 mm and a diameter of 5 mm (see **Fig. 2d**). The yield stress and tensile stress of the screws are 340 MPa and 420 MPa, respectively, as provided by the manufacturer. The screws have hexagonal heads, which are placed inside the short pipe, and the other end is drilled into wood. The four short pipes correspond to the four screws to increase the redundancy if one or two screws are cut off. The long pipe is embedded in the concrete block so that the steel bar in the concrete block can pass through this pipe. With this design, the long pipe works together with the concrete block. A length of 300 mm also prevents the pipe from pulling out from the concrete. This novel shear connector design is designed to provide sufficient redundancy and good overall performance, making the connector safe even if it experiences considerable shear force.

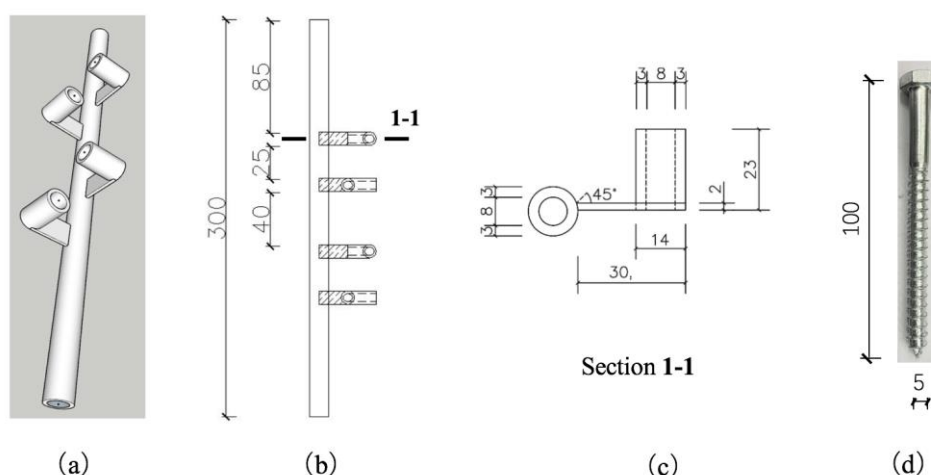


**Fig. 2.** Geometric information of the shear connector (unit: mm): (a) Three-dimensional diagram, (b) Plane dimensions, (c) Section 1-1, and (d) Screw dimensions

## 2.2 Wood properties

The timber member used in this study is made of spruce–pine–fir wood. Thirty 20 mm × 20 mm × 20 mm samples from the same batch were tested under axial compression, as shown in **Fig. 3a**. Fifteen samples were tested parallel to the grain, and the rest of the samples were tested perpendicular to the grain. Because wood has anisotropic properties, the samples present different failure modes between these two directions. The typical failure mode of samples tested parallel to the grain is buckling at the middle (see **Fig. 3b**). The samples perpendicular to the grain fail via inter-fiber gliding and cracking (see **Fig. 3c**).

Because the wood used in the push-out test is mainly under compression, only the sample test on the compression elastic modulus is carried out. During the sample test, displacement and force are measured from sensors. The strain is obtained from the ratio of displacement to the original length of the sample. **Table 1** summarizes the statistical results of the wood properties. Both the elastic modulus

and compressive stress parallel to the grain are much greater than those perpendicular to the grain. Due to the limited samples, the analysis results also indicate a high degree of scatter, with the coefficient of variation (c.o.v) ranging from 5.06% to 25.55%.

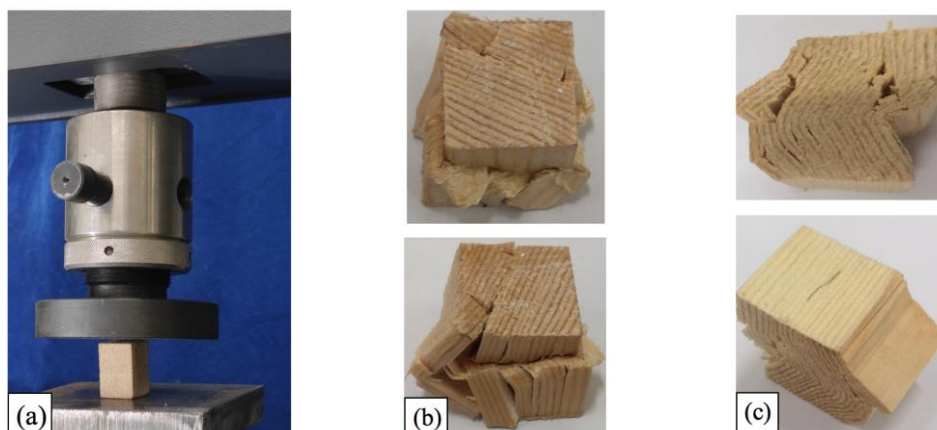


**Fig. 3.** Wood material testing: (a) Test setup, (b) Parallel-to-grain failure mode, and (c) Perpendicular-to-grain failure mode

**Table 1.** Statistical analysis of the wood properties

Directions	Elastic modulus		Compressive stress	
	Mean	c.o.v. (%)	Mean	c.o.v. (%)
Parallel to grain (MPa)	7970.99	25.55	30.67	8.91
Perpendicular to grain (MPa)	254.38	10.43	6.83	5.06

### 2.3 Concrete block properties

To obtain the characteristics of the concrete blocks, ten cubic specimens with dimensions of 150 mm × 150 mm × 150 mm were manufactured. After 28 days of curing, each sample was subjected to a compression test under a hydraulic actuator, as shown in **Fig. 4a**. Cracking on the surface of the concrete block was the typical failure mode (see **Fig. 4b**).

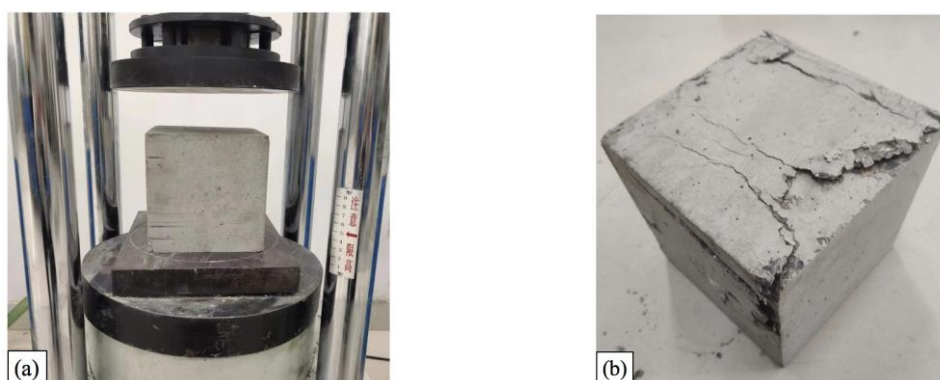


**Fig. 4.** Compression test of a concrete block: (a) Specimen and (b) Failure mode

**Table 2.** Material properties of the concrete

ID	Mass (kg)	Density (kg/m <sup>3</sup> )	Compressive strength (MPa)	ID	Mass (kg)	Density (kg/m <sup>3</sup> )	Compressive strength (MPa)
01	7.92	2346.67	44.8	06	7.88	2334.81	42.3
02	8.10	2400.00	44.0	07	7.96	2358.52	42.8
03	7.96	2358.52	47.0	08	8.50	2518.52	47.6
04	7.80	2311.11	44.2	09	7.86	2328.89	46.2
05	8.06	2388.15	45.9	10	7.94	2352.59	43.2

The material properties of the concrete are listed in **Table 2**. The ten plain concrete blocks have an average mass of 8 kg with a standard deviation of 0.19 kg. The average density of the samples was  $2369.78 \text{ kg/m}^3$  with a standard deviation of  $55.49 \text{ kg/m}^3$ . The compressive strength of each specimen ranged from 42.3 MPa to 47.6 MPa. The average compressive strength was 44.80 MPa, and the corresponding coefficient of variation was 3.84%

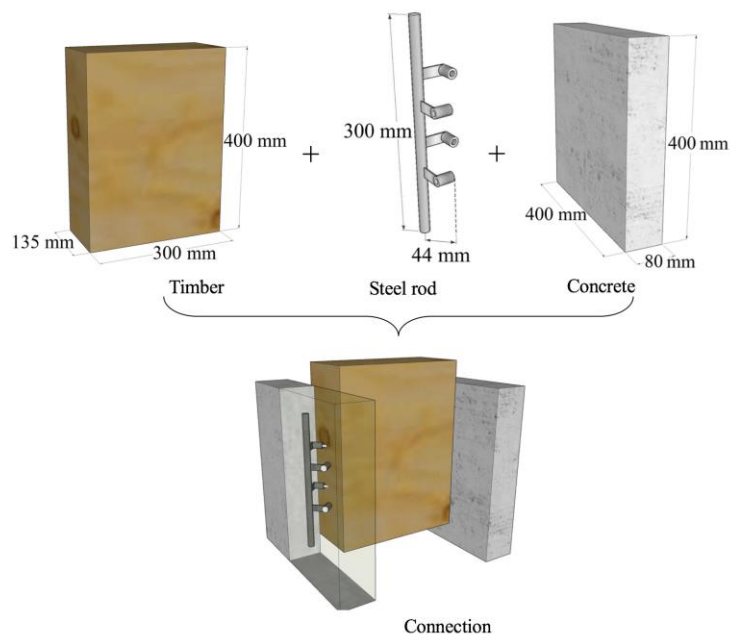


**Fig. 5.** Different components of a TCC connection



**Fig. 6.** Fabrication of a TCC connection: (a) Preparation of the components, (b) Screw driven into the hole, (c) Screws tapped into the plywood, (d) Setup of plywood formwork, and (e) Completed TCC connection

### 3. Push-out test

#### 3.1 Test specimens

The TCC connection consists of an  $80 \text{ mm} \times 400 \text{ mm} \times 400 \text{ mm}$  concrete block, two timber

members with dimensions of 135 mm × 300 mm × 400 mm and two shear connectors, as shown in **Fig. 5**. For the consideration of experimental variables, ten reduplication specimens were manufactured, which were labeled successively as T01 to T10. The fabrication of the TCC connection is illustrated as follows (see **Fig. 6**): First, eight holes are predrilled into two sides of the timber member (see **Fig. 6a**). On each side of the timber member, the steel tube is connected through four screws (see **Fig. 6b**). To ensure the tightness of the screw inside the hole, the screw is again gently tapped with a hammer, as shown in **Fig. 6c**. Once this is completed, the plywood formwork is set up on both sides of the timber member (see **Fig. 6d**). Then, the ready-mixed concrete is poured into the voids of the formwork around the steel tube, and a vibrator is used to settle the mixture. After 28 days of curing, the formwork is taken apart, and the manufacturing process of the TCC connection is completed (see **Fig. 6e**).

### 3.2 Test setup

The push-out test of the TCC connection was conducted under a hydraulic machine with a maximum capacity of 500 kN. **Fig. 7** displays a specimen used during the test. The specimen was placed on the top of a fixed bracket. For uniform loading, a single servo-hydraulic actuator was directly loaded above the midspan of a steel rectangular beam. Then, the applied load was transmitted to the wood member of the TCC connection. The loading protocol was displacement control with a constant rate of 1.6 mm/min. The loading was stopped either when the load capacity had reduced to 75% of the maximum load capacity or when the specimen had been completely destroyed. The loading was continuously recorded using the actuator itself. The displacement of the wood component was measured by the actuator itself, and the movement of the concrete components was measured by displacement transducers. The slip between wood and concrete components is equivalent to wood displacement minus concrete displacement.



**Fig. 7.** Push-out test setup

## 4 Failure modes and mechanical properties

### 4.1 Failure modes

The tested load-slip curves of the TCC connections are reported in **Fig. 8**. The ten curves are quite similar before the slip reaches 5 mm. This is because the specimen deformed elastically without any damage. As the load increased, splitting appeared between the wood laminates and increased in both length and width (see **Fig. 9a**). At this stage, the screws inside the specimens started to yield, and some differences were observed in the load-slip curves. As loading continued, a significant drop in load capacity occurred. This was attributed to the fracturing of the screw inside the wood component. The test was stopped when the load capacity was reduced to 75% of the maximum load capacity. Two typical load-slip curves are plotted in **Fig. 8b**, showing some difference. This occurred because wood properties are highly variable, and the manufacturing process of TCC connections includes some uncertainties. During the whole loading process, the concrete block exhibited no damage, and the wood component split along the direction of the wood grain. The interface between the concrete block and wood component presented slipping and cracking failure (see **Fig. 9b**). This behavior occurred because the concrete and timber components transmitted shear force through their interface.

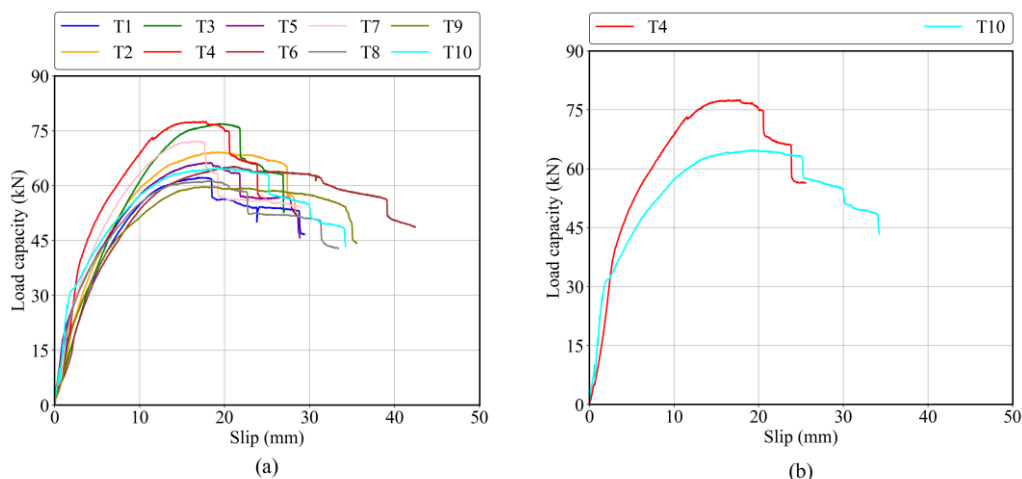


Fig. 8. Tested load-slip curves: (a) Ten specimens and (b) Two typical specimens

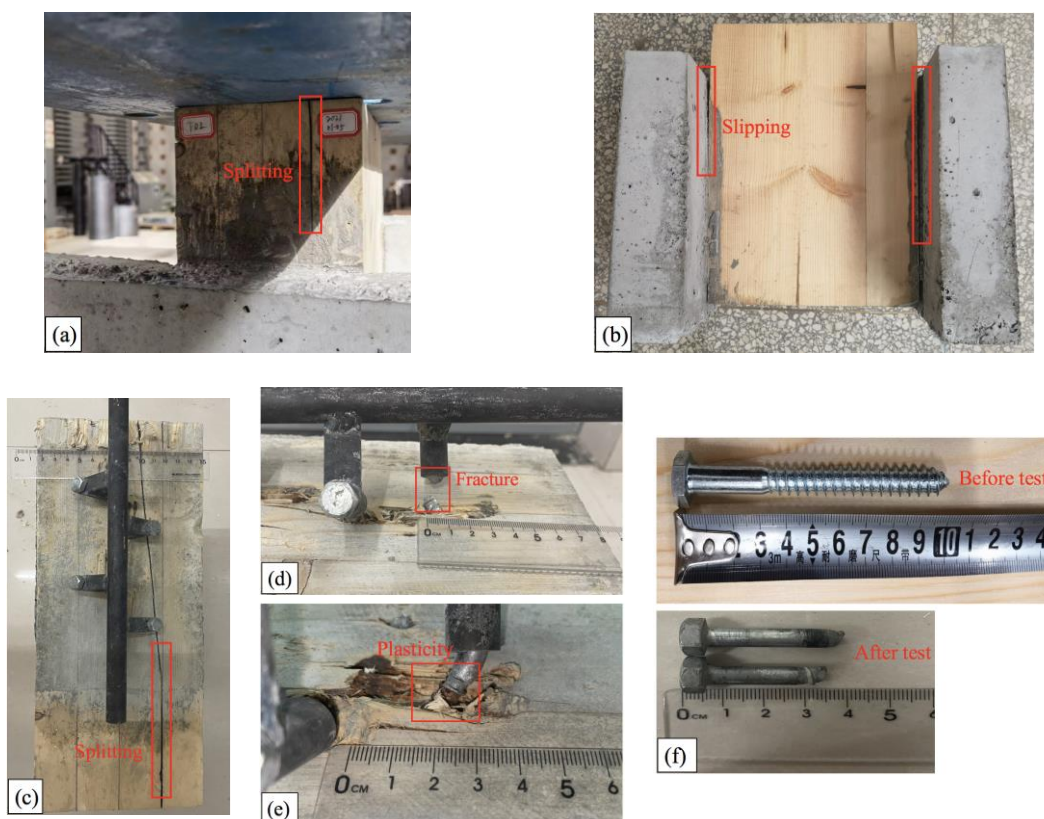


Fig. 9. Failure modes: (a) Wood splitting, (b) Interface slipping, (c) Wood surface splitting, (d) Screw fracturing, (e) Screw plastic deformation, and (f) Comparison of screws before and after testing

To further investigate the failure modes of different components, the TCC connection shown in Fig. 9a removed the concrete component; the failure mode of the wood component is presented in Fig. 9c. There was a clear 1-mm-wide split through the surface of the wood, and the steel tube remained intact. The screw acting as a connector between the steel tube and timber exhibited two failure modes: fracturing (Fig. 9d) and plastic failure (Fig. 9e). As shown in Fig. 9d, the screw was fractured a short distance into the timber, and the wood around the screw experienced severe crushing. The screw in Fig. 9e exhibits excessive plasticity, accompanied by wood crushing within a distance of 2 mm to 3 mm. Fig. 9f compares the condition of screws before and after testing. The screw was fractured 3-4 cm from the head. This fracture occurred at the surface, initiating in the smooth area and extending to the threaded area. Fig. 9 (c)-(e) shows different failure modes on different specimens, showing that the

manufacturing process for TCC connections, including some uncertainties, could influence failure modes.

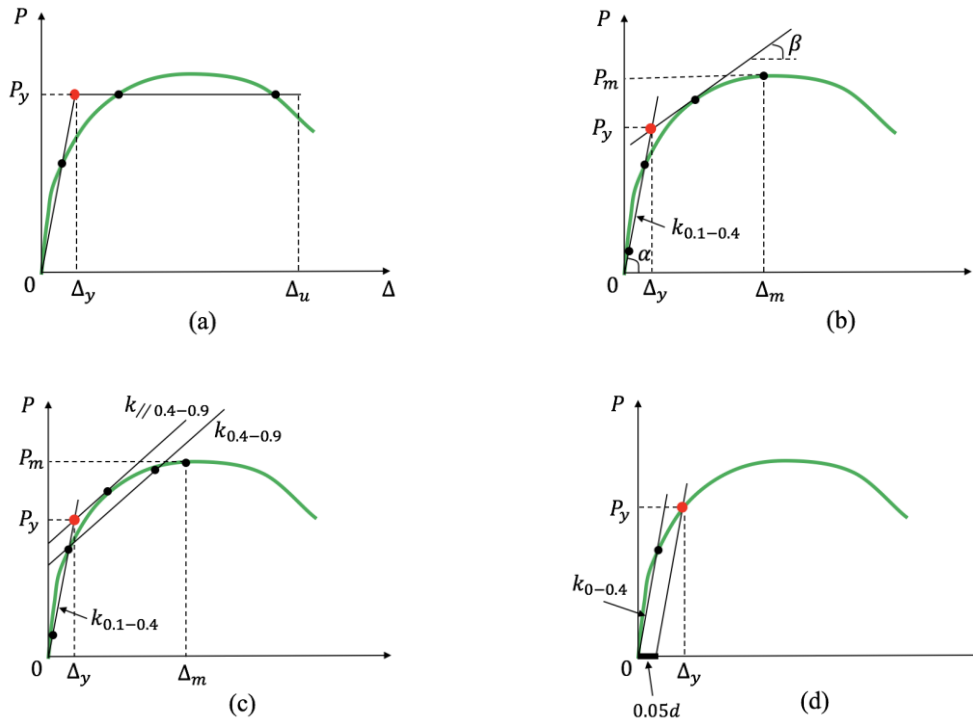


Fig. 10. Methods of yield point determination: (a) EEEP, (b) CEN, (c) Y&K, and (d) 5% diameter

#### 4.2 Analysis of mechanical properties

The tested load-slip curves of TCC connections do not have a clear yield platform, and it is difficult to determine the yield point. Some researchers have proposed several useful means to obtain the yield point, as noted in Fig. 10. The first tool is called the equivalent energy elastic–plastic curve (EEEE) [34]. A perfect elastic–plastic curve has an initial stiffness and a horizontal line (see Fig. 10a). The initial stiffness is defined as the secant slope of origin and 40% of the maximum load capacity. According to the bilinear curve, the yield load ( $P_y$ ) is calculated by

$$P_y = \left[ \Delta_u - \sqrt{\Delta_u^2 - \frac{2E_u}{k_{0-0.4}}} \right] k_{0-0.4} \quad (1)$$

in which  $E_u$  is the sum of energy dissipation to the ultimate slip ( $\Delta_u$ ). The ultimate slip is determined by the corresponding ultimate load capacity; the ultimate load capacity is defined as the largest value between 80% of the maximum load capacity and the failure point.  $k_{0-0.4}$  is the initial stiffness defined by the secant of origin and 40% of the maximum load capacity ( $P_m$ ).

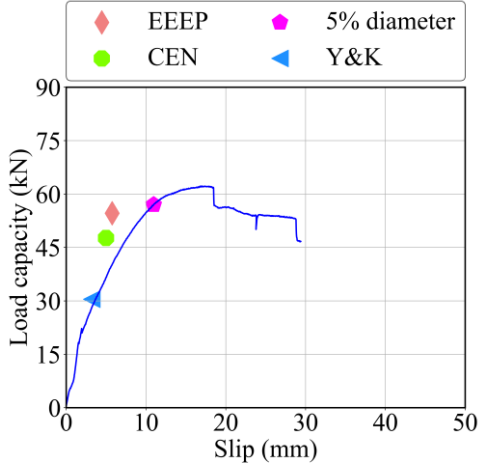
The determination of the yield point given by the European Committee of Standardization (CEN) is also a popular method [35]. For this method, the yield point (red point in Fig. 10b) is the intersection of two lines. The first line is the secant slope of 10% and 40% of the maximum load capacity denoted by  $\alpha$ . The second line whose slope ( $\beta$ ) should be satisfied with  $\tan \beta = (\tan \alpha)/6$  is tangent to the load-slip curve.

The third method was proposed by Yasumura and Kawai (Y&K) [36]. A secant line between 10% and 40% of the peak load is defined. Another straight line is determined by the tangent to the load-slip curve, whose slope is parallel to the secant line between 40% and 90% of the peak load. The intersection of the two lines is regarded as the yield point (see Fig. 10c).

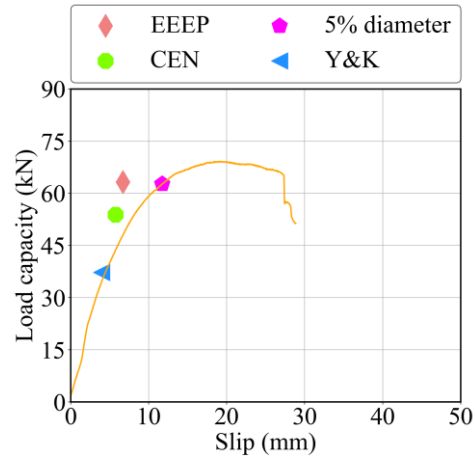
Fig. 10d depicts the yield point determined by a 5% diameter (named 5% diameter) [37]. A straight line that is defined by 0% and 40% of the peak load is extracted initially. This straight line offsets to 5%

of the connector diameter, making it intersect with the load-slip curve. This intersection point represents the yield point.

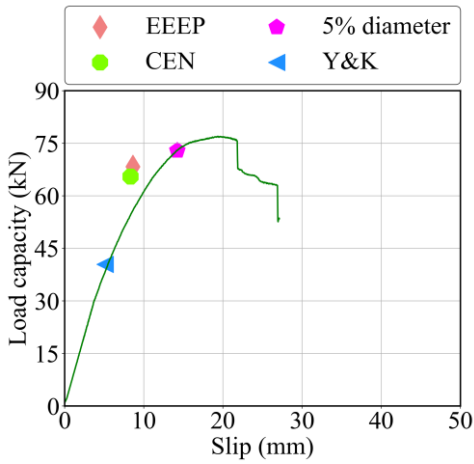
According to the above four methods for the determination of the yield point, **Fig. 11** compares the locations of yield points obtained using different methods for each specimen. The yield points determined by Y&K and 5% diameter lie in the load-slip curve, while the yield points calculated using the other two approaches offset the curve.



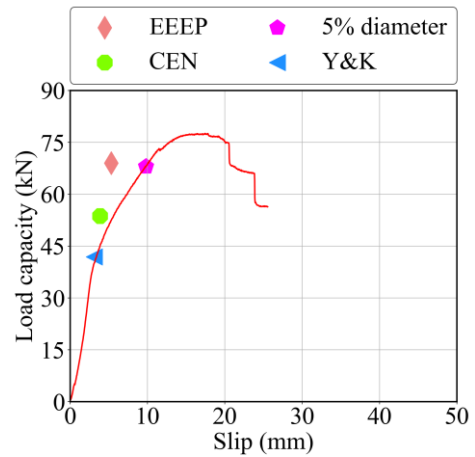
(a) Specimen T1



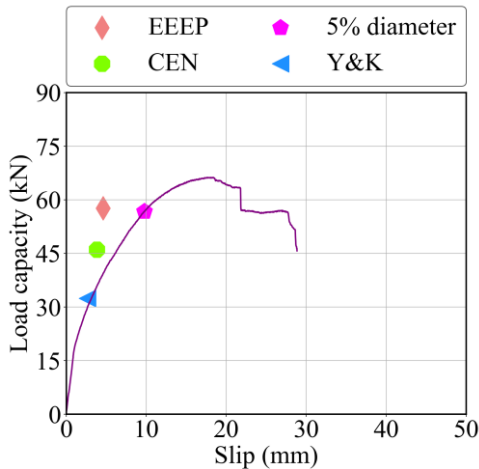
(b) Specimen T2



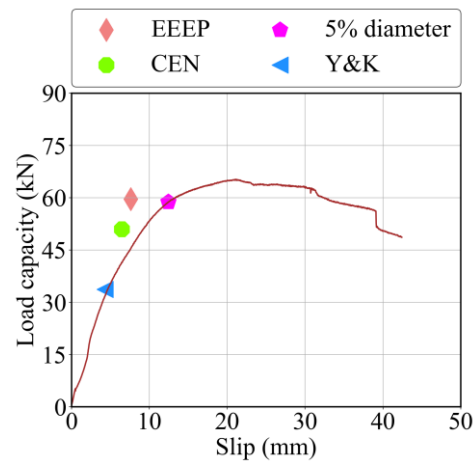
(c) Specimen T3



(d) Specimen T4



(e) Specimen T5



(f) Specimen T6

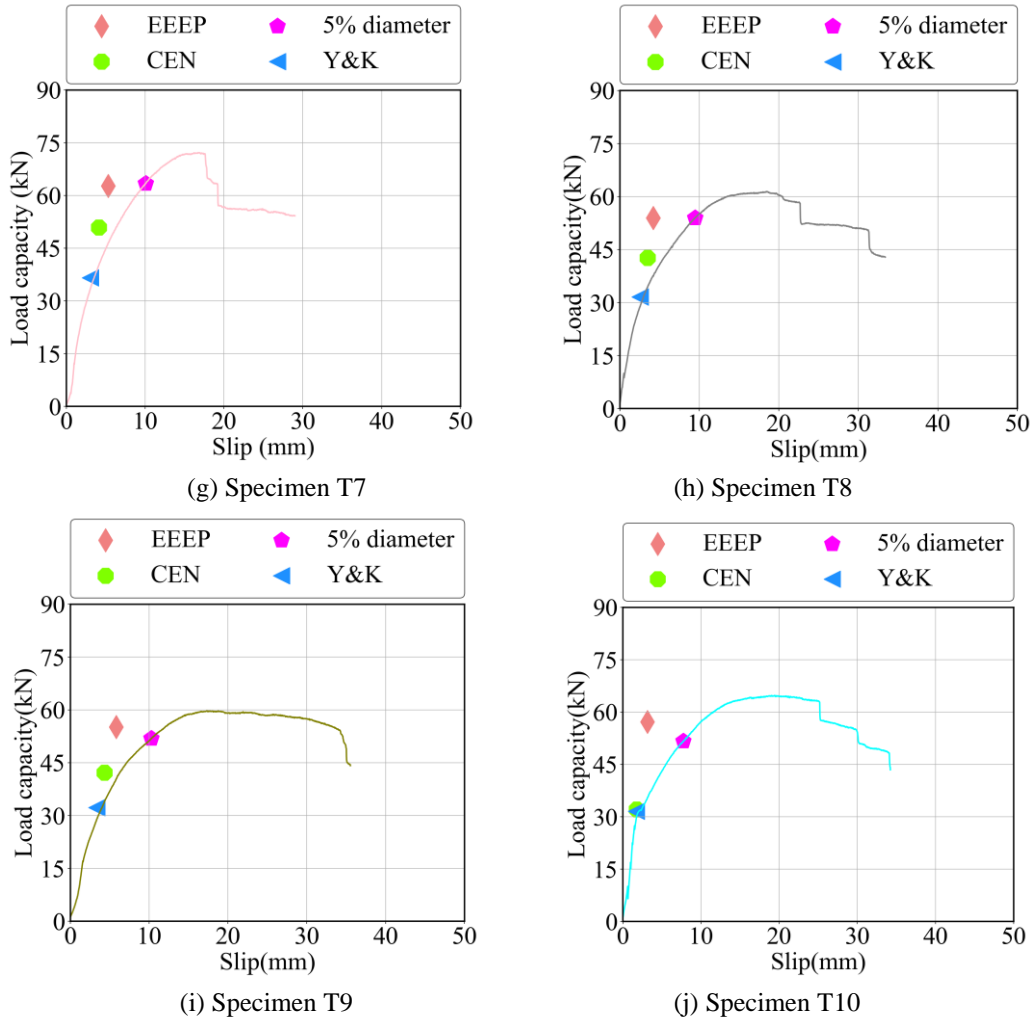


**Fig. 11.** Tested load-slip curves and yield points determined by four methods

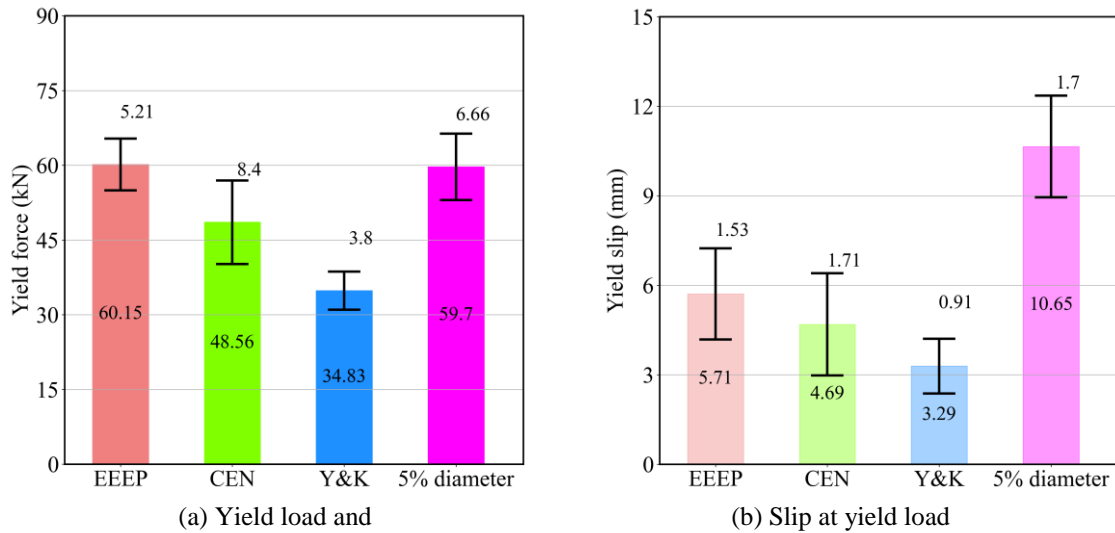


**Fig. 12.** Tested load-slip curves and yield points determined by four methods

Taking the statistical analysis of yield points, **Fig. 12** displays the mean values of yield points associated with standard deviation. The yield load and corresponding slip determined by the Y&K method are the lowest among the four methods. The peak load has a significant influence on the yield point under the Y&K method. Both the EEEP method and 5% diameter method have almost the same yield force, yet the 5% diameter method has approximately twice as much yield slip as the EEEP method. The reason is that the EEEP method assesses the yield point from the area enclosed by the load-slip

curve, whereas the 5% diameter considers the influence of the connector. The yield load and corresponding slip determined by the CEN method are larger than values determined by the Y&K method but lower than the values determined by the EEEP and 5% diameter methods. Due to limited test data, it is difficult to determine which method is best suited to determine the yield points of TCC connections. The comparison results in this study will help researchers and engineers better understand the advantages and disadvantages of these four methods.

For the initial stiffness, the methods of EEEP and 5% diameter take the slope between 0% and 40% of the peak point. Both the CEN and Y&K methods define the straight line between 10% and 40% of the peak load as an initial stiffness. The reason for starting from 10% of the peak load is that this considers the influence of initial consolidation. Due to the geometric roughness of the predrilled holes in the timber, the wood and screw may have imperfect contact, leading to low stiffness. **Fig. 13** compares the calculated initial stiffness obtained using four different approaches. The values of initial stiffness calculated by the four methods are almost the same. This means that the TCC connections have a marginal initial slip that can be ignored.

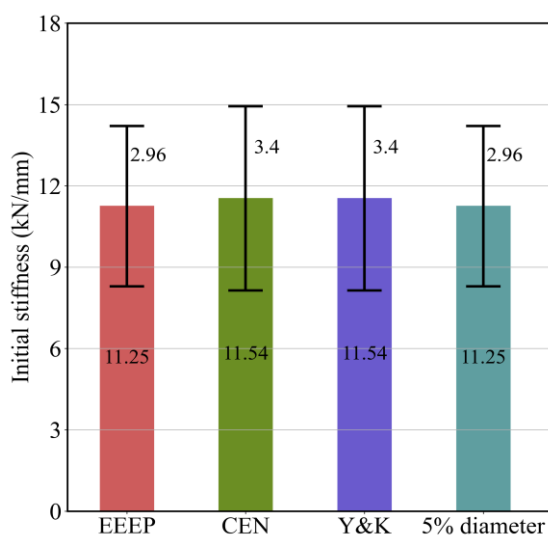


**Fig. 13.** Comparison of initial stiffness values obtained using different methods

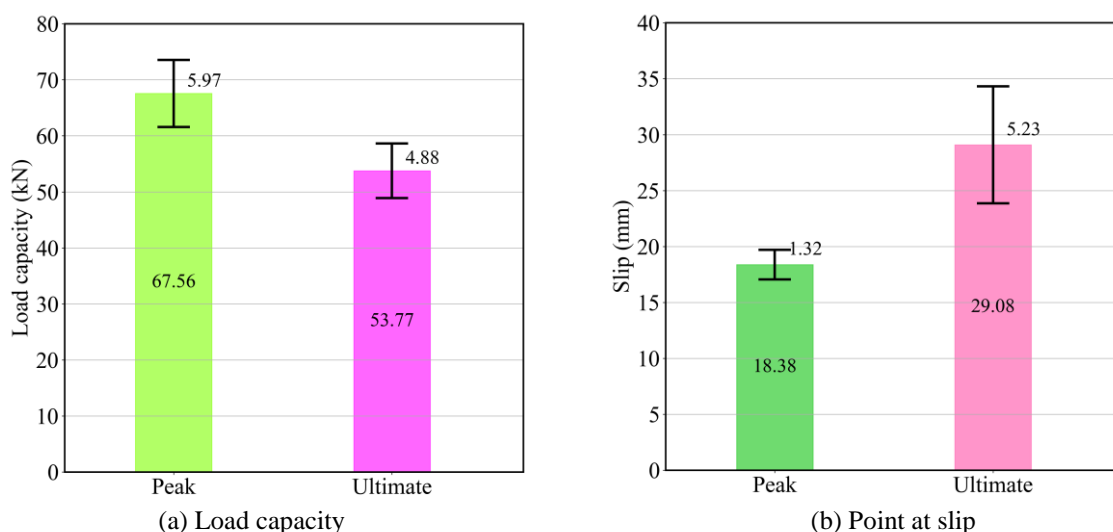


**Fig. 14.** Statistic analysis on peak point and ultimate

For each specimen, the peak point is the maximum load capacity and its corresponding slip. The ultimate load is defined as either the failure load or 80% of the peak load. The average values of the peak and ultimate load capacity are 67.56 kN and 53.77 kN, respectively, as noted in **Fig. 14a**. Their corresponding standard deviations are 5.97 kN and 4.88 kN, respectively (**Fig. 14b**). For the slip, the average values at the peak point and ultimate point are 18.38 mm and 29.08 mm, respectively. The slip

is 10.7 mm between the peak point and ultimate point, which is 58.22% of the slip at the peak point. This indicates that the TCC connections have strong ductility.

Compared to traditional TCC connections, the TCC connections with novel connectors perform better. In reference [33], the TCC connections for the notch without rods and the rod without notches have a maximum load-carrying capacity of 18.0-30.8 kN. In reference [39], timber-concrete bolted connections without steel pads have an initial stiffness of 2.36-4.56 kN/mm and a maximum load-carrying capacity of 18.87-26.82. These values are smaller than the corresponding mechanical properties reported in this study. This further demonstrates that the proposed TCC connections have good performance over other traditional TCC connections.

## 5. Analytical model and parameter uncertainty evaluation

### 5.1 Bayesian formulation for a regression problem

The mechanical properties of the TCC connections have been comprehensively investigated from test results, yet an analytical load-slip model is usually required in the design and analysis of TCC structures. A preferred model describing the load-slip curve is one with few parameters related to mechanical properties [39][40]. Therefore, an empirical load-slip model based on Foschi's model [41] and Cao's model [42] is proposed.

$$P = P_{\max} \left[ 1 - \exp\left(-\frac{k_e}{P_{\max}} \Delta\right) \right], 0 \leq \Delta \leq \Delta_{\max} \quad (2)$$

where  $k_e$  is the elastic stiffness,  $P_{\max}$  and  $\Delta_{\max}$  are the maximum load capacity and corresponding displacement, respectively, and  $P$  and  $\Delta$  are the predicted load and corresponding slip, respectively.

This model describes the nonlinear load-slip curves up to the maximum load. It involves three parameters, of which  $P_{\max}$  and  $\Delta_{\max}$  can be easily collected from the peak point of the load-slip curve. The value of  $k_e$  is determined by the slope of the asymptotes trending to zero. Compared to other models, one of the distinct features of this model is that all the model parameters have clear physical meanings, which is user-friendly for engineers hoping to identify the values of parameters from load-slip curves.

Even if an analytical model is available, determining model parameters is still a major challenge. Because wood properties vary greatly, the mechanical properties of TCC connections present large differences even if they are the same types of connections. The use of the probability method to describe results is more appropriate than using the determined values. To address these issues, Bayesian inference provides a good paragon with which to estimate the model parameters as well as their uncertainties [43]. Eq. (2) can be rewritten as a more general expression:

$$Y = f(\mathbf{X}, \boldsymbol{\theta}) + \varepsilon \quad (3)$$

in which  $f(\mathbf{X}, \boldsymbol{\theta})$  is the nonlinear function,  $\boldsymbol{\theta} = [k_e, P_{\max}]$  are model parameters,  $\mathbf{X}$  is the slip regarded as the predictor (or independent variable),  $Y$  is the corresponding predicted force (or dependent variable), and  $\varepsilon$  is a prediction error.

From the Bayesian view, Eq. (3) can be expressed in terms of probability distributions,

$$Y \sim N(f(\mathbf{X}, \boldsymbol{\theta}), \sigma^2) \quad (4)$$

in which symbol  $Y$  in Eq. (4) is interpreted as a random variable following a Gaussian distribution with mean  $f(\mathbf{X}, \boldsymbol{\theta})$  and variance  $\sigma^2$ . According to Eq. (4), the Bayesian formalism reformulates a parameter fitting problem as a search for a probability distribution, as shown in **Fig. 15**. This distribution can be sampled using Markov chain Monte Carlo (MCMC) methods [44]. The basic idea of MCMC methods is to draw samples from a probability distribution. As the target probability distribution is usually unknown, a useful technique is to sample from a known probability density that is proportional to the target function. The properties of the collected samples (e.g., expected value and variance) are used to evaluate the characteristics of the target distribution. A detailed description can be found in

Ravenzwaaij et al. [45].

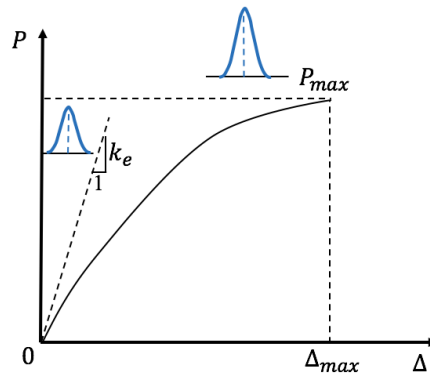


**Fig. 15.** Mathematical model with parameter distributions

## 5.2 Analysis results

In the estimation process, ten sets of test data are stochastically divided into two groups: one for regression analysis and the other for cross validation. **Fig. 16** displays the tested load-slip curves of the regression and validation groups, and the data exceeding the maximum load capacity are not considered hereafter because Eq. (2) can only simulate the load-slip curves up to the maximum load.

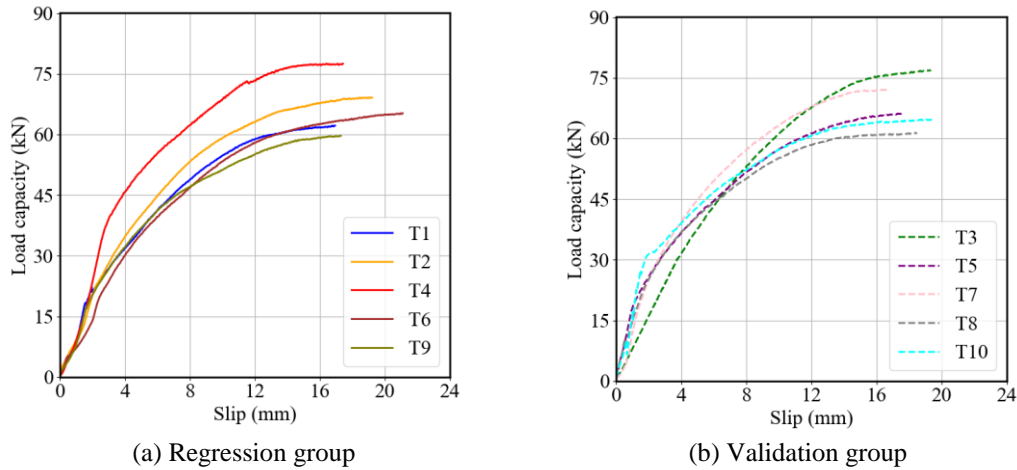


**Fig. 16.** Two groups of test data

According to Eq. (3), two parameters  $\theta = [k_e, P_{max}]$  are selected to be identified. Both parameters are assumed to follow a Gaussian distribution, whose mean and standard deviation are extracted from the regression group (see Table 3). Prediction error  $\epsilon$  follows an exponential probability density function with a mean value of 5.2. Then, the MCMC algorithm is performed to draw samples from the posterior distribution. As the first few hundred points may be unrelated to the final distribution of interest, the first 1000 samples are burned in, and the remaining 7000 samples are used to infer the posterior distribution.

**Table 3.** Prior distribution of estimated parameters

Parameter	Mean	Standard deviation
$k_e$ (kN/mm)	11.54	2.89
$P_{max}$ (kN)	66.79	6.99

**Fig. 17a** and **Fig. 18a** record the individual samples of parameters  $k_e$  and  $P_{max}$ , respectively, at each step. Both chains have no major drifts or odd patterns. This means that each sampling chain converges well and is stationary. To further infer what the posterior distribution of each parameter looks like, the histograms of sample data are plotted (see **Fig. 17b** and **Fig. 18b**). The x-axis shows the values of each parameter, and a probability on the y-axis indicates how likely the parameter value is. To estimate the shape of the unknown density function, kernel density estimation (KDE) was used to

smooth the histograms of the sampled data. The KDE plots of both the stiffness and maximum load capacity present a Gaussian-like distribution.

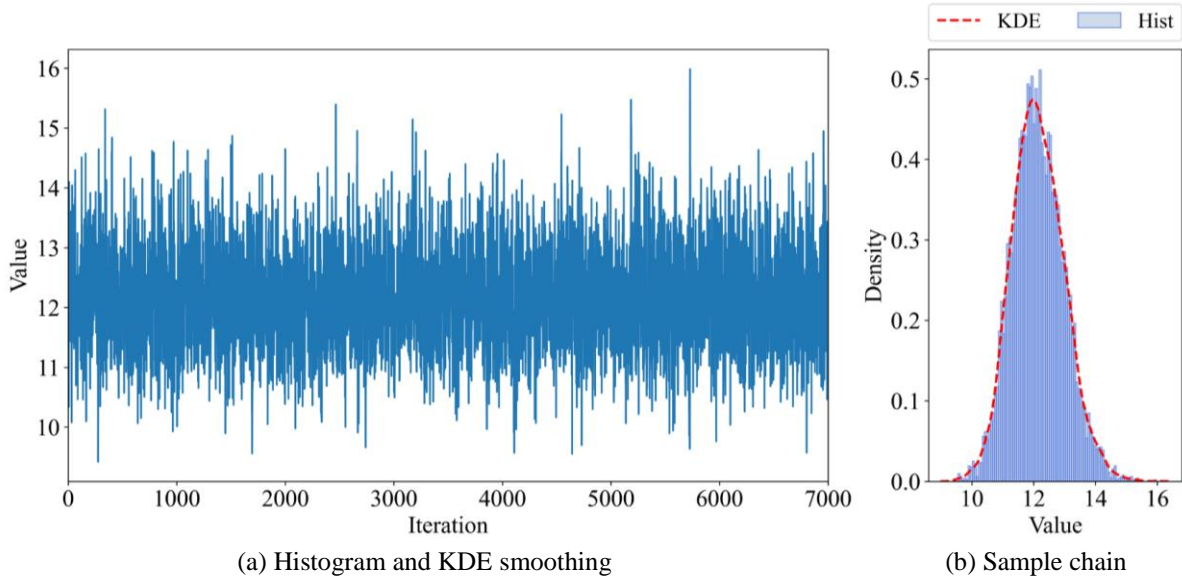


**Fig. 17.** Posterior estimate of parameter  $k_e$

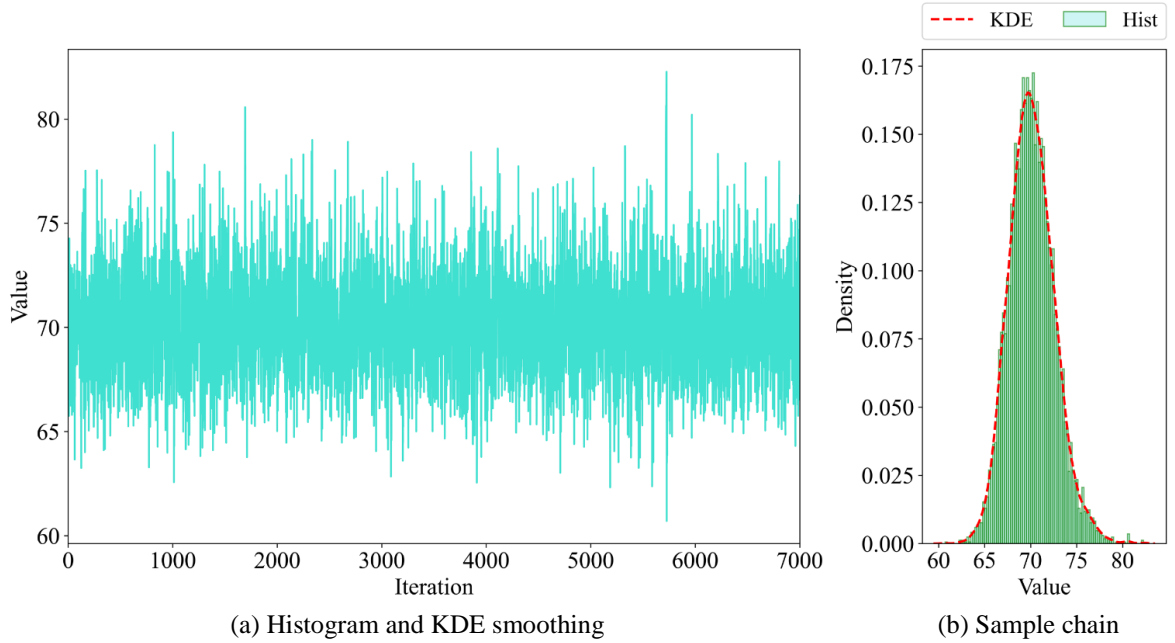


**Fig. 18.** Posterior estimate of parameter  $P_{max}$

**Table 4.** Statistical properties of the estimated parameters

Parameter	Mean	Standard deviation	HDI-3%	HDI-97%
$k_e$ (kN/mm)	12.139	0.846	10.662	13.786
$P_{max}$ (kN)	70.192	2.472	65.796	74.995

From **Fig. 17** and **Fig. 18**, one can calculate the statistics of the posterior distribution for each parameter, as reported in **Table 4**. Compared to the standard deviation in **Table 3**, that in **Table 4** is much smaller. This is because the new information provided by the test data reduces uncertainty regarding the parameter distribution. Another advantage of performing Bayesian inference is that the uncertainty of parameters can be quantified using the highest density interval (HDI) [46]. The interval between HDI-3% and HDI-97% represents the 94% most credible values for a parameter. Taking parameter  $k_e$  in **Table 4** as an example, there is a 94% probability that the value is between 10.662

kN/m and 13.786 kN/m.

When the probability model for load-slip curves is attained, it is important to conduct a validation that checks how well the models capture the data. For this purpose, 5000 sets of  $k_e$  and  $P_{\max}$  are produced from the posterior distribution of the estimated parameters. Then, these sets of parameters are fed into the analytical model (i.e., Eq. (2)) generating the load-slip curves. The synthetic data for load-slip curves are depicted by the light blue areas in **Fig. 19**. This area becomes large in the overall trend as the value of slip increases. To test how predictive the model is in terms of the estimated parameters, **Fig. 19** also plots five validation sets. The five tested curves lie in the light blue area within a slip of 8 mm. When the value of slip exceeds 8 mm, two test curves are outside the light blue area. This occurs because only limited test data lead to a considerable amount of uncertainty in the estimate results. When more test data are available, the Bayesian method has the advantage of incorporating test data into the priority distribution to enhance the a posteriori probability. This means that the reliability of the estimated distribution can be improved.

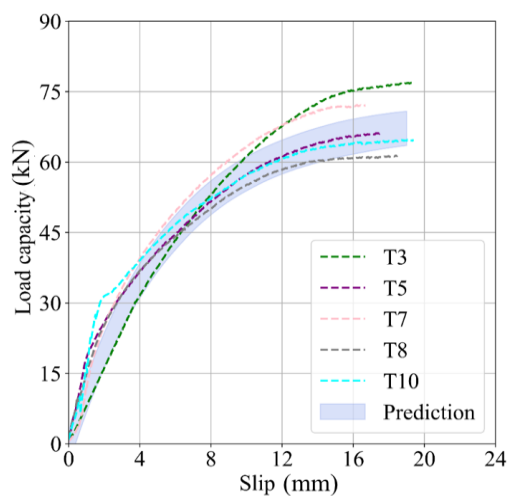


**Fig. 19.** Cross-validation of the prediction results.

## 6 Discussion

It should be noted that only the type of shear connectors is investigated in this work. Screw numbers, screw length and spaces between neighboring short pipes may influence the performance of TCC connections, but they are not studied herein. The objective is to design a novel shear connector that makes the composite connection between timber and concrete work more effectively. Some preliminary work has been done to explore the shear performance of this novel connection. For the composite connection, the connector between two different components usually transmits the shear force, easily resulting in a failure. The developed TCC connections with novel connectors perform better in initial stiffness and maximum load-carrying capacity than conventional TCC connections [33][39]. This indicates that the novel TCC connections show potential for application in TCC structures. To obtain better performance from the novel connector, more work on the optimization of the geometric dimension of a long pipe and four short pipes will be done in the future. A regression of the tested load-slip curves using the Bayesian formulation is performed to predict the load capacity of the TCC considering uncertainty. Since this type of connection only repeats ten sets of data, the Markov chain Monte Carlo technique is employed to generate data. If more test data become available, they can be incorporated into the estimated results, and the estimated uncertainty will in turn be improved.

## 7 Conclusion

This paper describes an experimental investigation of TCC connections. Ten push-out tests, in which novel shear connectors are proposed, are conducted to verify the mechanical properties of the proposed TCC connection. The Bayesian method is introduced to estimate the model parameters with

the test data and quantify the uncertainty of the model parameters. Several conclusions attained from this work are given as follows:

(1) The novel shear connector can effectively transmit the shear force to the interface. The failure mode was wood cracking, and no connector was sheared off in any of the connections.

(2) The test results indicate that composite connections with novel shear connectors are high in initial stiffness, are high in maximum load-carrying capacity, and show good ductility compared to traditional connections.

(3) The Bayesian method is applied to estimate the parameters of a mathematical model based on test data and to quantify the uncertainty of model parameters. The obtained results are useful for reliability analysis.

### Availability of data and materials

Most data analyzed during this study are included in this published article. Supplementary information is available from the corresponding author on reasonable request.

### Competing interests

The authors declare that they have no known competing financial interests or personal relationships that could have appeared to influence the work reported in this paper.

### Authors' contributions

**Yingyang Liu:** Methodology, Investigation, Writing - original draft, Funding acquisition. **Ao Li:** Software, Visualization. **Jixing Cao:** Conceptualization, Formal analysis, Writing - review & editing. **Dan Yu:** Data curation, Resources. **Jilu Zhang:** Data curation.

### Acknowledgements

This paper is funded by the Open Program of Henan Key Laboratory of Grain and Oil Storage Facility & Safety (Grant No. 2021KF-B01) and the 2022 Students' Innovation and Entrepreneurship Training Program of Zhengzhou University.

### References

- [1] Su J, Li H, Xiong Z, Lorenzo R. Structural design and construction of an office building with laminated bamboo lumber. *Sustain Struct* 2021; 1(2): 000010. <https://doi.org/10.54113/j.sust.2021.000010>.
- [2] Chiniforush A A, Valipour H R, Bradford M A, Akbarnezhad A. Long-term behaviour of steel-timber composite (STC) shear connections. *Engineering Structures* 2019; 196: 1. <https://doi.org/10.1016/j.engstruct.2019.109356>.
- [3] Li X, Ashraf M, Subhani M, Ghabraie K, Li H, Kremer P. Withdrawal resistance of self-tapping screws inserted on the narrow face of cross laminated timber made from Radiata Pine. *Structures* 2021; 31: 1130-1140. <https://doi.org/10.1016/j.istruc.2021.02.042>.
- [4] Dauletbek A, Li H, Xiong Z, Lorenzo R. A review of mechanical behavior of structural laminated bamboo lumber. *Sustain Struct* 2021; 1(1): 000004. <https://doi.org/10.54113/j.sust.2021.000004>.
- [5] Crawford R H, Cadorel X. A framework for assessing the environmental benefits of mass timber construction. *Procedia engineering* 2017; 196: 838-846. <https://doi.org/10.1016/j.proeng.2017.08.015>.
- [6] Tannert T, Moudgil M. Structural design, approval, and monitoring of a UBC tall wood building. *Structures Congress 2017; 2017: 541-547*. <https://doi.org/10.1061/9780784480410.045>.
- [7] Malo K A, Abrahamsen R B, Bjertnæs M A. Some structural design issues of the 14-storey timber framed building "Treet" in Norway. *European Journal of Wood and Wood Products* 2016; 74(3): 407-424. <https://doi.org/10.1007/s00107-016-1022-5>.
- [8] Tlustochowicz G, Serrano E, Steiger R. State-of-the-art review on timber connections with glued-in steel rods. *Materials and structures* 2011; 44(5): 997-1020. <https://doi.org/10.1617/s11527-010-9682-9>.
- [9] Zhu W, Yang H, Liu W, Shi B, Ling Z, Tao H. Experimental investigation on innovative connections for timber-concrete composite systems. *Construction and Building Materials* 2019; 207: 345-356. <https://doi.org/10.1016/j.conbuildmat.2019.02.079>.
- [10] Djoubissie D D, Messan A, Fournely E, Bouchair A. Experimental study of the mechanical behavior of

- timber-concrete shear connections with threaded reinforcing bars. *Engineering Structures* 2018; 172: 997-1010. <https://doi.org/10.1016/j.engstruct.2018.06.084>.
- [11] Chybiński M, Polus Ł. Experimental and numerical investigations of aluminium-timber composite beams with bolted connections. *Structures* 2021; 34: 1942-1960. <https://doi.org/10.1016/j.istruc.2021.08.111>.
  - [12] Boccadoro L, Zweidler S, Steiger R, Frangi A. Bending tests on timber-concrete composite members made of beech laminated veneer lumber with notched connection. *Engineering Structures* 2017; 132: 14-28. <https://doi.org/10.1016/j.engstruct.2016.11.029>.
  - [13] Shi B, Liu W, Yang H, Ling X. Long-term performance of timber-concrete composite systems with notch-screw connections. *Engineering Structures* 2020; 213: 110585. <https://doi.org/10.1016/j.engstruct.2020.110585>.
  - [14] Zhang L, Chui Y H, Tomlinson D. Experimental investigation on the shear properties of notched connections in mass timber panel-concrete composite floors. *Construction and Building Materials* 2020; 234: 117375. <https://doi.org/10.1016/j.conbuildmat.2019.117375>.
  - [15] Taazount M, Amziane S, Molard D. Tangential behavior of nailed composite timber-concrete floor structures. *Construction and Building Materials* 2013; 40: 506-513. <https://doi.org/10.1016/j.conbuildmat.2012.09.092>.
  - [16] Navaratnam S, Herath N, Lokuge W, Thamboo J, Poologanathan K. Performance of timber girders with end-notch: Experimental and numerical investigation. *Structures* 2021; 29: 730-740. <https://doi.org/10.1016/j.istruc.2020.11.075>.
  - [17] Cao J, Xiong H, Wang Z, Chen J. Experimental investigation and numerical analysis for concrete-CLT connections. *Construction and Building Materials* 2020; 236: 117533. <https://doi.org/10.1016/j.conbuildmat.2019.117533>.
  - [18] Kanócz J, Bajzecerová V, Šteller Š. Timber-concrete composite elements with various composite connections. Part 1: Screwed connection. *Wood research* 2013; 58(4): 555-570.
  - [19] Sebastian W M, Piazza M, Harvey T, Webster T. Forward and Reverse shear transfer in beech LVL-concrete composites with singly inclined coach screw connectors. *Engineering Structures* 2018; 175: 231-244. <https://doi.org/10.1016/j.engstruct.2018.06.070>.
  - [20] Otero-Chans D, Estévez-Cimadevila J, Suárez-Riestra F, et al. Experimental analysis of glued-in steel plates used as shear connectors in Timber-Concrete-Composites. *Engineering Structures* 2018; 170: 1-10. <https://doi.org/10.1016/j.engstruct.2018.05.062>.
  - [21] Sebastian W M. Switch from connection ductility to reinforcement ductility with curvature reversal in timber-concrete composites. *Construction and Building Materials* 2019; 229: 116886. <https://doi.org/10.1016/j.conbuildmat.2019.116886>.
  - [22] Negrão J H J O, Leitão de Oliveira C A, Maia de Oliveira F M, Paulo Barreto Cachim. Glued composite timber-concrete beams. I: Interlayer connection specimen tests. *Journal of Structural Engineering* 2010; 136(10): 1236-1245. [https://doi.org/10.1061/\(ASCE\)ST.1943-541X.0000228](https://doi.org/10.1061/(ASCE)ST.1943-541X.0000228).
  - [23] Brunner M, Romer M, Schnüriger M. Timber-concrete-composite with an adhesive connector (wet on wet process). *Materials and structures* 2007; 40(1): 119-126. <https://doi.org/10.1617/s11527-006-9154-4>.
  - [24] Eisenhut L, Seim W, Köhlborn S. Adhesive-bonded timber-concrete composites—Experimental and numerical investigation of hygrothermal effects. *Engineering Structures* 2016; 125: 167-178. <https://doi.org/10.1016/j.engstruct.2016.05.056>.
  - [25] Fu Q, Yan L, Thielker N A, Kasal B. Effects of concrete type, concrete surface conditions and wood species on interfacial properties of adhesively-bonded timber-Concrete composite joints. *International Journal of Adhesion and Adhesives* 2021; 107: 102859. <https://doi.org/10.1016/j.ijadhadh.2021.102859>.
  - [26] Cao J, Xiong H, Liu Y. Experimental study and analytical model of bolted connections under monotonic loading. *Construction and Building Materials* 2021; 270: 121380. <https://doi.org/10.1016/j.conbuildmat.2020.121380>.
  - [27] Cao J, Xiong H, Wang Z, Chen J. Mechanical characteristics and analytical model of CLT-concrete composite connections under monotonic loading. *Construction and Building Materials* 2022; 335: 127472. <https://doi.org/10.1016/j.conbuildmat.2022.127472>.
  - [28] Hassanieh A, Valipour H R, Bradford M A. Composite connections between CLT slab and steel beam: Experiments and empirical models. *Journal of Constructional Steel Research* 2017; 138: 823-836. <https://doi.org/10.1016/j.jcsr.2017.09.002>.
  - [29] Dias A, Martins A R D, Simoes L M C, Providência P M, Andrade A A M. Statistical analysis of timber-concrete connections—Mechanical properties. *Computers & Structures*, 2015, 155: 67-84. <https://doi.org/10.1016/j.compstruc.2015.02.036>.
  - [30] Cao J, Xiong H, Chen L. Procedure for parameter identification and mechanical properties assessment of CLT connections. *Engineering Structures* 2020; 203: 109867. <https://doi.org/10.1016/j.engstruct.2019.109867>.
  - [31] Liu P, Au S K. Bayesian parameter identification of hysteretic behavior of composite walls. *Probabilistic Engineering Mechanics* 2013; 34: 101-109. <https://doi.org/10.1016/j.probengmech.2013.08.005>.

- [32] Cao J, Xiong H, Chen J. Mechanical performance of timber-concrete bolted connections under cyclic loading. *Structures* 2021; 34: 3464-3477. <https://doi.org/10.1016/j.istruc.2021.09.086>.
- [33] Djoubissie D D, Messan A, Fournely E, Bouchaïr A. Experimental study of the mechanical behavior of timber-concrete shear connections with threaded reinforcing bars. *Engineering Structures* 2018; 172: 997-1010. <https://doi.org/10.1016/j.engstruct.2018.06.084>.
- [34] American Society for Testing and Materials (ASTM). 2005a. ASTM E 2126-05. Standard Test Method for Cyclic (Reversed) Load Test for Shear Resistance of Walls for Buildings. Annual Book of ASTM Standards. ASTM, West Conshohocken, PA, USA.
- [35] EN 12512. Timber structures—test methods—cyclic testing of joints made with mechanical fasteners. CEN, Brussels, Belgium, 2001.
- [36] Yasumura, M., and N. Kawai. Estimating seismic performance of wood-framed structures. *Proceedings of 5th WCTE 1998*; 2: 564-571.
- [37] American Society for Testing and Materials (ASTM). 2005b. ASTM D 5764-97a. Standard Test Method for Evaluating Dowel-Bearing Strength of Wood and Wood-Based Products. Annual Book of ASTM Standards. ASTM, West Conshohocken, PA, USA.
- [38] Cao J, Xiong H, Peng T. Load-carrying capacity analysis for timber-concrete bolted connections considering the effect of steel pads. *Engineering Structures* 2021; 247: 113095. <https://doi.org/10.1016/j.engstruct.2021.113095>.
- [39] Dong H, He M, Wang X, Christopoulos C, Li Z, Shu Z. Development of a uniaxial hysteretic model for dowel-type timber joints in OpenSees. *Construction and Building Materials* 2021; 288: 123112. <https://doi.org/10.1016/j.conbuildmat.2021.123112>.
- [40] Cao J, Xiong H, Zhang F L, Chen L, Cazador C R. Bayesian model selection for the nonlinear hysteretic model of CLT connections. *Engineering Structures* 2020; 223: 111118. <https://doi.org/10.1016/j.engstruct.2020.111118>.
- [41] Ricardo O. Foschi. Analysis of wood diaphragms and trusses. Part I: Diaphragms. *Canadian Journal of Civil Engineering* 1977; 4(3): 345-352. <https://doi.org/10.1139/177-043>.
- [42] Cao J, Liu Y, Wang Y, Zhang Y. Load-slip performance of timber-to-concrete connections with U-steel connectors under push-out test. *Journal of Building Engineering* 2022; 45: 103527. <https://doi.org/10.1016/j.jobe.2021.103527>.
- [43] Beck J L. Bayesian system identification based on probability logic. *Structural Control and Health Monitoring* 2010; 17(7): 825-847. <https://doi.org/10.1002/stc.424>.
- [44] Gamerman D, Lopes H F. Markov chain Monte Carlo: stochastic simulation for Bayesian inference. CRC Press 2006.
- [45] Van Ravenzwaaij D, Cassey P, Brown S D. A simple introduction to Markov Chain Monte-Carlo sampling. *Psychonomic bulletin & review* 2018; 25(1): 143-154. <https://doi.org/10.3758/s13423-016-1015-8>.
- [46] Makowski D, Ben-Shachar M S, Lüdtke D. bayestestR: Describing effects and their uncertainty, existence and significance within the Bayesian framework. *Journal of Open Source Software* 2019; 4(40): 1541. <https://doi.org/10.21105/joss.01541>.